Multilayer diffractive optical element material selection method based on transmission, total internal reflection, and thickness

Laborde, Victor ; Loicq, J.J.D.; Hastanin, Juriy ; Habraken, Serge

DOI
10.1364/AO.465999

Publication date
2022

Document Version
Final published version

Published in
Applied Optics

Research Article Vol. 61, No. 25 / 1 September 2022 / Applied Optics 7415

applied optics

Multilayer diffractive optical element material selection method based on transmission, total internal reflection, and thickness

Victor Laborde,[1,*] Jérôme Loicq,[1,2] Juriy Hastanin,[1] and Serge Habraken[1]

[1]Centre Spatial de Liege, University of Liège, Avenue du Pré-Aily, 4031 Angleur, Belgium
[2]Faculty of Aerospace Engineering, Delft University of Technology, Kluyverweg 1, 2629 HS Delft, The Netherlands
*Corresponding author: victor.laborde@uliege.be

Received 6 June 2022; revised 28 July 2022; accepted 9 August 2022; posted 11 August 2022; published 24 August 2022

The polychromatic integral diffraction efficiency (PIDE) metric is generally used to select the most suitable materials for multilayer diffractive optical elements (MLDOEs). However, this method is based on the thin element approximation, which yields inaccurate results in the case of thick diffractive elements such as MLDOEs. We propose a new material selection approach, to the best of our knowledge, based on three metrics: transmission, total internal reflection, and the optical component's total thickness. This approach, called "geometric optics material selection method" (GO-MSM), is tested in mid-wave and long-wave infrared bands. Finite-difference time-domain is used to study the optical performance (Strehl ratio) of the "optimal" MLDOE combinations obtained with the PIDE metric and the GO-MSM. Only the proposed method can provide MLDOE designs that perform. This study also shows that an MLDOE gap filled with a low index material (air) strongly degrades the image quality.

https://doi.org/10.1364/AO.465999

1. INTRODUCTION

Earth observation in the thermal infrared (IR) bandwidth addresses numerous issues, particularly in the security and surveillance domains. According to the reviews in [1,2], most IR applications require only two distinct bandwidths: agriculture, irrigation monitoring, forest fires detection, etc. In these cases, expensive multispectral spaceborne instruments can be replaced by smaller dual-band instruments. Atmospheric IR windows define IR wave bands: the mid-wave IR (MWIR) from 4.4 to 5 μm (to avoid solar reflections) and the long-wave IR (LWIR) from 8 to 12 μm. Due to the low number of transmissive IR materials, this wide discontinuous wave band generates huge chromatic aberrations that are hard to come by for refractive systems. However, some IR glass manufacturers now provide alternatives to the classical zinc selenide (ZnSe), zinc sulfide (ZnS), and germanium (Ge) materials: the chalcogenides [3], which have lower refractive indices, lower hardness, and moldable properties.

When combined with refractive lenses, diffractive lenses [diffractive optical elements (DOEs)] make very efficient achromat solutions but cannot operate efficiently in both MWIR and LWIR wave bands. Accordingly, innovative diffractive lenses, called multilayer DOEs (MLDOEs), were introduced in 1997 [4], extending the diffractive lenses' behavior for multiple wavelengths. MLDOEs are made of two harmonic diffractive layers [5,6] [harmonic DOEs (HDOEs)] separated by air (two-layer DOE) or by another material (three-layer DOE). The number of possible material combinations is huge when chalcogenide materials are included, requiring a specific material selection procedure. The diffraction efficiency is a standard performance metric associated with diffractive optics, most of the time calculated using the thin element approximation (TEA). In the frame of this analytical theory, the diffraction efficiency of MLDOEs reaches over 95% in the whole MWIR-LWIR bandwidth for on-axis incidence and any material combination [7,8]. On the other hand, off-axis incidence studies [9–11] have shown that an increase of the incident angle results in a loss of diffraction efficiency, which depends on the material combination. A widely used material selection method (MSM) [12] is based on the following observation: an "optimal" MLDOE design should undergo the smallest diffraction efficiency drop for the highest incidence angle. Although this method is fast and gives useful results, its applicability is limited by the validity domain of the TEA. The latter becomes progressively inaccurate when the heights of the diffractive microstructures increase. For MLDOEs, they are, by design, 100 times higher than in the case of classical mono-layer DOEs. More recently, geometric approaches have been used to perform more accurate computations of diffractive efficiency [13,14] and optical phase modeling [15,16].

This paper proposes a new MSM based on three evaluation metrics: transmission, total internal reflection (TIR), and total

MLDOE thickness. According to this alternative approach, an "optimal" MLDOE design should provide the highest amount of transmission with the lowest TIR and thickness. In the following, we refer to this material selection procedure as the "geometric optics MSM" (GO-MSM), since it is based on ray-tracing and Fresnel equations to assess the TIR and the MLDOE transmission. The GO-MSM provides an MLDOE material selection but does not directly evaluate the image quality of selected MLDOEs. To validate this approach and compare its result with the existing polychromatic integral diffraction efficiency (PIDE) MSM (PIDE-MSM), we use rigorous finite-difference time-domain (FDTD) electromagnetic calculations. The optical performance of an MLDOE design is determined by the Strehl ratio, computed at the "best" focal plane. The Strehl ratio is retrieved based on FDTD near-field calculation and Fourier optics, as detailed in [16].

The TEA-based PIDE-MSM is recalled and applied in Section 2 and provides a first MLDOE material selection result. The proposed GO-MSM is then described in Section 3. Various optimal material selections are made for two-layer DOEs (Section 4.A) and three-layer DOEs (Section 4.B). Finally, performance evaluations (Strehl ratio) are provided at the focal plane for the best designs of each method (Section 5) and discussed in Section 6.

2. PIDE MATERIAL SELECTION METHOD

A. MLDOE Design Equations and PIDE Definition

MLDOEs are composed of two HDOEs [5,6] (Fig. 1), joined together by an optical material or separated by air. These HDOEs are made of different materials, and their groove heights are designed to provide constructive interferences for two distinct wavelengths, called "design wavelengths" and denoted λ_1 and λ_2. In this paper, we selected $\lambda_1 = 4.7\ \mu$m and $\lambda_2 = 10.4\ \mu$m, based on the wavelength selection method [8] applied in the same time in MWIR and LWIR. Both layers are aligned and have the same groove periods (i.e., same number of diffractive zones). Each MLDOE zone can be approximated by the N-step structure of Fig. 1.

Figure 1 is used to compute the optical path differences (OPDs) for both layers 1 and 2, with an off-axis incidence. The calculation, described in detail in [11], leads to the analytical

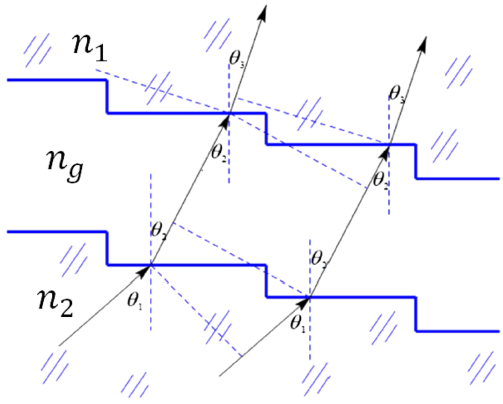

Fig. 1. Ray propagation inside an MLDOE for off-axis incident angle [12]. The continuous surfaces of each layer are modeled with an N-step profile instead.

expression of total off-axis phase delay for MLDOEs:

$$\Phi(\lambda,\theta) = H_1\left[n_1(\lambda)\cos\theta - \sqrt{n_g^2(\lambda) - n_1^2(\lambda)\sin^2\theta}\right] + H_2\left[\sqrt{n_2^2(\lambda) - n_1^2(\lambda)\sin^2\theta}\right], \tag{1}$$

where n_1, n_2, and n_g are respectively the refractive indices of layers 1 and 2 and the gap. H_1 and H_2 are the respective microstructure heights for layers 1 and 2. Their expression can be obtained from Eq. (1) under the conditions of constructive interferences for the two design wavelengths λ_1 and λ_2, for the first diffractive order, and considering normal incidence:

$$\begin{cases} H_1 = \frac{\lambda_2 A(\lambda_1) - \lambda_1 A(\lambda_2)}{B(\lambda_1)A(\lambda_2) - B(\lambda_2)A(\lambda_1)}, \\ H_2 = \frac{\lambda_1 B(\lambda_2) - \lambda_2 B(\lambda_1)}{B(\lambda_1)A(\lambda_2) - B(\lambda_2)A(\lambda_1)} \end{cases}, \tag{2}$$

where $A(\lambda) = n_2(\lambda) - n_g(\lambda)$ and $B(\lambda) = n_1(\lambda) - n_g(\lambda)$. The most valuable evaluation metric is PIDE [17]: it is the integral of the diffraction efficiency over the considered wave band. It is based on the angle-dependent phase expression [Eq. (1)], and written for the mth diffractive order as

$$\eta(\theta, m) = \frac{1}{\lambda_{\max} - \lambda_{\min}} \int_{\lambda_{\min}}^{\lambda_{\max}} \operatorname{sinc}^2\left(m - \frac{\Phi(\lambda,\theta)}{2\pi}\right) d\lambda, \tag{3}$$

where $\lambda_{\max}$ and $\lambda_{\min}$ represent the boundary wavelengths of the considered wave band. The total IR PIDE is the weighted sum of two PIDEs, one calculated in MWIR and the other in LWIR. We consider only the first diffractive order, as it is the main operating order for MLDOEs:

$$\eta(\theta, 1) = \frac{1}{2}\left[\eta_{\mathrm{MWIR}}(\theta, 1) + \eta_{\mathrm{LWIR}}(\theta, 1)\right]. \tag{4}$$

The PIDE depends on the incident angle, the chosen wave bands, and most importantly, the MLDOE material combination. Note that the term "MLDOE material combination" represents a triplet of material (m_1, m_g, m_2). The denominations "two-layer DOE" and "three-layer DOE" are employed when the gap material m_g is filled by air or another IR material.

B. Results of the PIDE-MSM

This section focuses on the application of the PIDE-MSM detailed in [10] and analyzes its potential limits. The variation of the PIDE with the incident angle is displayed in Figs. 2(a) and 2(b) for multiple MLDOE combinations.

Figure 2(a) displays the best two-layer DOE combinations, according to [10]: only the 10 MLDOEs with the highest PIDE at maximal incidence (15°) are shown. The air gap is imposed for manufacturing reasons since linking two HDOEs with an IR material can be difficult. Figure 2(a) shows an important diffraction efficiency drops when the incidence increases. All 10 combinations start with >95% PIDE for on-axis incidence and end with PIDE values between [65–85]% PIDE 15° incidence, except for the IRG24-air-IRG25 combination (97% PIDE).

Similar to Fig. 2(a), Fig. 2(b) displays the 10 best three-layer DOEs combinations. Any IR gap material is considered, regardless of the feasibility of the resulting MLDOEs. All

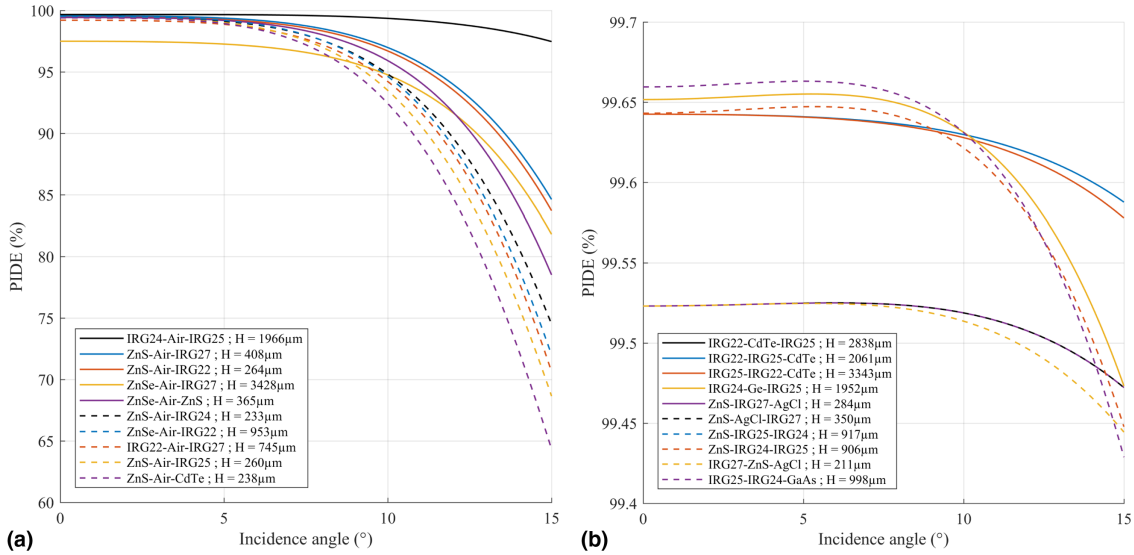

Fig. 2. Angle-dependent PIDE for various MLDOE configurations: (a) two-layer DOEs and (b) three-layer DOEs. The two layers and the gap materials are variables in (b), while an air gap is imposed in (a). Only the 10 configurations with maximal PIDE at 15° incidence are plotted. The PIDE variations are similar to [10]. H represents the total MLDOE thickness, computed using Eq. (2).

the solutions depicted in Fig. 2(b) have negligible efficiency decreases (the worst PIDE being 99.4% at 15°). Since no thickness metric is accounted for in the PIDE method [10], we define IRG22-IRG25-CdTe as an optimal three-layer DOE for the PIDE-MSM.

It results from this analysis that the on-axis PIDE is nearly independent of the material combination since it is above 95% for all combinations depicted in Figs. 2(a) and 2(b). This behavior results from Eq. (1) and the choice of design wavelengths: for any material combination, an MLDOE will always provide 100% diffraction efficiency at the design wavelengths $\lambda_{1,2}$, assuming the TEA is valid.

C. Limits of the PIDE Method

In the general frame of scalar diffraction theory (SDT), the most employed scalar approximation for diffractive optics design is the TEA. It considers infinitely thin elements and gives analytical expressions in the calculus of optical path length (OPL) and phase delays. According to [18], the TEA is valid when three restrictions are met:

- the diffractive feature sizes of the micro-structure are much larger than the wavelength;
- the field is paraxial;
- the micro-structure is thin.

For any diffractive element, including the MLDOE, the diffractive zone periods are designed following [19]:

$$r_m^2 = 2mf\lambda_{1,2} = 2mF/\#D\lambda_{1,2}, \tag{5}$$

with f the focal length, D the aperture diameter, and $F/\#$ the f-number. The integer $m \in [1, N]$ corresponds to the zone number, where N is the total number of zones. $\lambda_{1,2}$ represents any of the two MLDOE design wavelengths ($\lambda_1 = 4.7$ µm and $\lambda_2 = 10.4$ µm). Generally speaking, the period size $T_m = r_m - r_{m-1}$ is always much larger than the maximum wavelength (at least 14 times is required [20]). However, considering the MLDOE design described in Section 2.A and the off-axis PIDE method, the "paraxial" and "thin element" requirements are not fulfilled. Even when on-axis PIDE is considered, according to [21], the aspect ratio of each layer and zone should remain smaller than 1/6. The aspect ratio $\mathcal{R}$ of the mth zone and layer i is defined as

$$\mathcal{R}(i, m) = \frac{H_i}{T_m}. \tag{6}$$

It has been shown in [16] that very few MLDOEs fulfilled the requirement $\mathcal{R}(i, m) < 1/6$, and only for very high f-numbers.

We take the most optimal two-layer MLDOE of Fig. 2(a) as an example: IRG24-air-IRG25. For standard values $N = 10$ and $F/\# = 15$, the period of the first zone is ∼3 mm. Following Eq. (2), each layer is ∼1 mm thick. The resulting aspect ratio is $\mathcal{R} = 0.33 > 1/6$, meaning that the TEA is not applicable for this f-number. An aspect ratio of 1/6 (for the first zone only) can be obtained with an F/30 design of aperture diameter $D = 19$ mm, keeping 10 diffractive zones. This example shows that only a very constraining MLDOE design can ensure the validity of the TEA, and only for the largest zone. If extreme zones (i.e., lowest period) are considered, the TEA cannot fulfill the "thin" restriction mentioned above.

Furthermore, applying GO laws to the IRG24-Air-IRG25 MLDOE shows that it has a huge transmission drop due to TIR: TIR occurs at the IRG24-air interface (refractive index ratio of 0.38) when an on-axis incident ray makes a 22.5° angle with the grooves' interface normal. It happens inside the first zone, starting from the radius $r = 0.48$ mm. As a result, only 10% of the MLDOE aperture can transmit light, leading to a nearly opaque MLDOE design. Therefore, the 100% on-axis diffraction efficiency predicted in Fig. 2(a) is very likely overestimated, considering an F/15 MLDOE design. This numerical analysis is

rigorously verified in Section 5, when studying the optical performance of the IRG24-air-IRG25 and IRG22-IRG25-CdTe solutions using FDTD.

In the following, we propose an alternative process based not on analytical diffraction efficiency but rather on GO. We recall that using ray-tracing and geometrical considerations to model diffractive elements is not new. A hybrid refractive–diffractive model was developed in [22] under the name "zone decomposition" modeling, further implemented in [23]. Field tracing [15] also uses ray-tracing to model microstructure interfaces. Finally, a ray-based phase model for MLDOEs has been used in [16], providing much more accurate results than the TEA.

3. GEOMETRIC OPTICS MATERIAL SELECTION METHOD

This section presents an alternative MLDOE MSM, based on GO, called the GO-MSM. The GO-MSM relies on three evaluation metrics: TIR, transmission at each interface, and total MLDOE thickness. These metrics can be calculated rapidly for any MLDOE design and incident angle, using a standard ray-tracing engine (ASAP in this paper [24]) and Eq. (2). According to the GO-MSM, the most "optimal" MLDOE combination has the highest transmission and the lowest TIR and thickness. In this paper, we present the on-axis selection process, and we provide the off-axis results in Appendix A because they do not bring any change in the results.

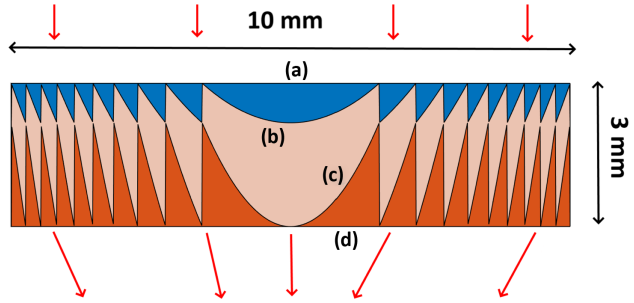

Fig. 3. Geometry and shape of an arbitrary selected MLDOE: IRG23-IRG22-IRG25. The top blue layer is IRG23, the gap (salmon color) is IRG22, and the bottom orange layer is IRG25. The red arrows display the incident light's direction. The optical interfaces are denoted: (a) layer 1 back, (b) layer 1 grooves, (c) layer 2 grooves, and (d) layer 2 back. The MLDOE was designed according to Section 2.A.

An example of geometric evaluation metric calculation is shown in Figs. 3 and 4. Figure 3 presents the shape and the different optical interfaces of an arbitrarily selected MLDOE (IRG23-IRG22-IRG25).

Figure 4 displays the transmission map, obtained with GO and Fresnel reflection equations, for each interface defined in Fig. 3.

Figure 4 shows the evolution of transmission and TIR inside the arbitrarily selected MLDOE. The TIR percentage metric consists of the area covered by TIR over the circular aperture area. In this particular example, the working portion of the MLDOE is composed of only the central zones, thus potentially reducing its performance. The average measure of TIR is defined as the maximal amount of TIR after all interfaces, in this case, 85%, while the average transmission equals 62%.

The presented evaluation metrics (TIR, transmission, and thickness) are used in multiple selection processes, considering two-layer DOEs in Section 4.A and three-layer DOEs in Section 4.B. The optimization variables are the layer/gap materials.

4. RESULTS OF THE GO-MSM

In this section, we use the proposed GO-MSM to provide a selection of MLDOE combinations for two and three-layer

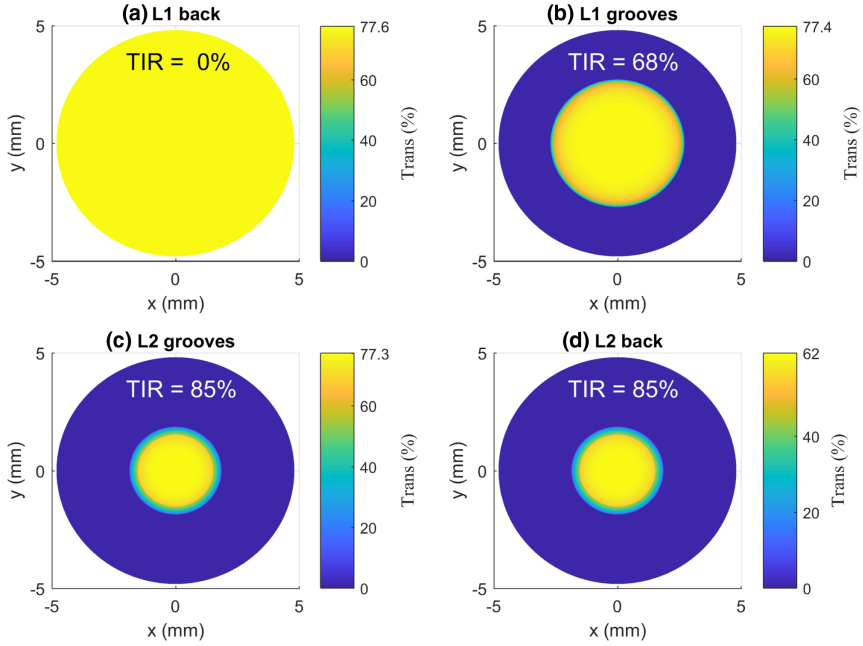

Fig. 4. Transmission map for each interface of the IRG23-IRG22-IRG25 MLDOE depicted in Fig. 3. The blue portion represents TIR (null transmission), whereas the white borders are outside the circular aperture.

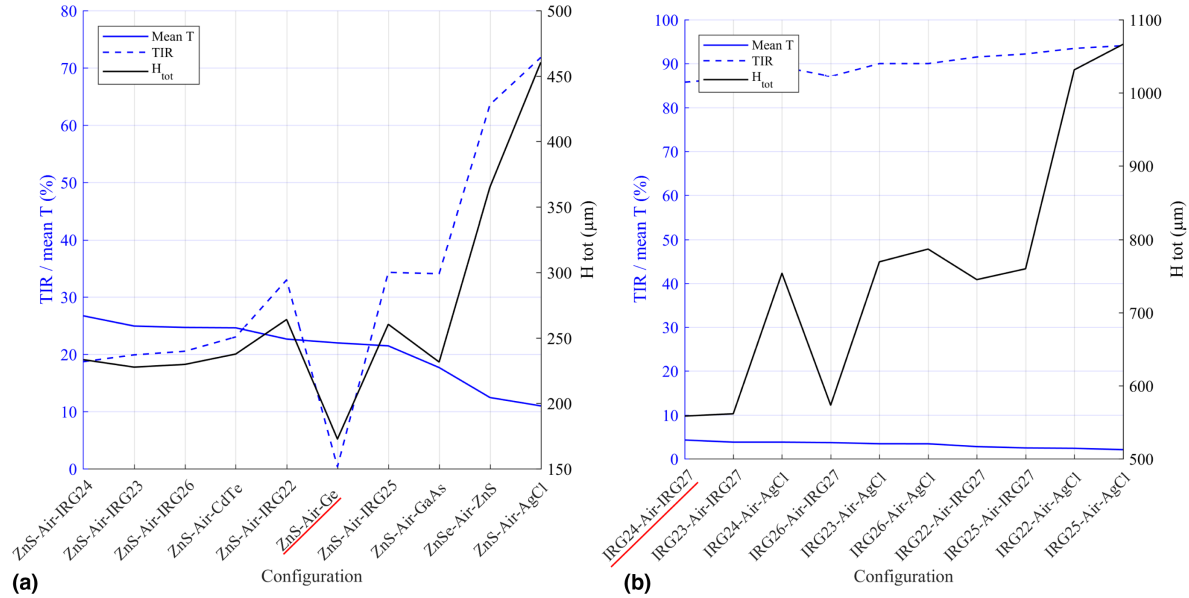

Fig. 5. On-axis geometric selection method results for the 10 "best" material configurations with an air gap. The design parameters are $D = 10$ mm, F/15, and $N = 10$. Three evaluation metrics are shown: transmission (blue line, left axis), TIR (blue dotted line, left axis), and thickness (black line, right axis). The best MLDOE combinations are underlined in red and correspond to the solutions with the lowest TIR and thickness and high transmission. (a) All IR materials and (b) "soft" materials.

DOEs. The validation of this method is performed in Section 5, using FDTD as a reference.

We fix the same design parameters as in Section 2.B: the $F/\#$ is set to 15 at $\lambda = 8$ μm, and the number of zones N is fixed to 10, giving an aperture radius $D = 10$ mm. These parameters are standard, providing a relatively small number of zones and aperture diameter, considering a potential manufacturing process.

In this paper, we denote IR materials as "hard" (ZnS, Ge, ZnSe, CdTe and GaAs) or "soft" (IRG22-27 and AgCl). This denotation comes from the relative hardness property of these materials. Since a softer material will likely be more easily manufactured, we perform the GO-MSM considering all IR materials or only the soft materials. These two analyses are made for two-layer DOEs and three-layer DOEs, resulting in four different optimization results.

A. Two-Layer DOE Optimal Configuration

The GO-MSM presented in Section 3 is applied in the case of two-layer DOEs. The gap is made of air, while the materials of both layers are variables. The results of the GO-MSM are presented in Figs. 5(a) and 5(b), respectively, for all IR materials and only soft materials.

Interestingly, Figs. 5(a) and 5(b) provide very different results. No combination from the soft only selection process [Fig. 5(b)] can effectively be used for an optical design: the average transmission is only 5%, while TIR is ∼90%. In this case, the best solution is IRG24-air-IRG27, displaying the lowest thickness.

In Fig. 5(a), while the material of the first layer is a variable, the final solutions are all made of ZnS-Air-X, showing that ZnS allows much better transmission (20%) and TIR values than chalcogenides do. Nevertheless, while ZnS seems to be a suitable material to be coupled with an air gap, except for the ZnS-Air-Ge configuration, the remaining possibilities are rather bad, displaying low transmission and high TIR. In addition, ZnS-Air-Ge is the only combination that generates no TIR, which coincides with its shallow thickness compared to the other solutions.

Contrary to the PIDE results of Fig. 2(a), where at least four configurations with air gaps had high imaging performance, even at 15° incidence, the result of the GO-MSM is much less optimistic. Note that the optimal configurations are different for the proposed GO-MSM and for the PIDE-MSM.

B. Three-Layer DOE Optimal Configuration

Three-layer DOEs need to be considered, to improve the performance, replacing the air gap with an IR material. We use the same method as in Section 4.A with a variable gap material and the same distinction between all IR materials and soft materials. The results are depicted in Fig. 6.

Figure 6 leads to much better solutions than Fig. 5. The optimal solution considering all IR materials [Fig. 6(a)] is ZnSe-ZnS-AgCl. It has the lowest thickness (195 μm), a relatively high transmission (57%), and null TIR. The best solution, obtained with only soft materials [Fig. 6(b)], is IRG24-IR27-AgCl. It has the same transmission value as the ZnSe-ZnS-AgCl solution, but a higher thickness (370 μm).

In Section 5, we derive the optical performance of all the presented solutions, for both PIDE and GO methods. We analyze whether the expected optical quality of the selected solutions matches their real performance.

5. VALIDATION OF THE GO-MSM: POLYCHROMATIC STREHL RATIO

This comparative section draws the image quality of the optimal solutions provided by the PIDE-MSM and the proposed

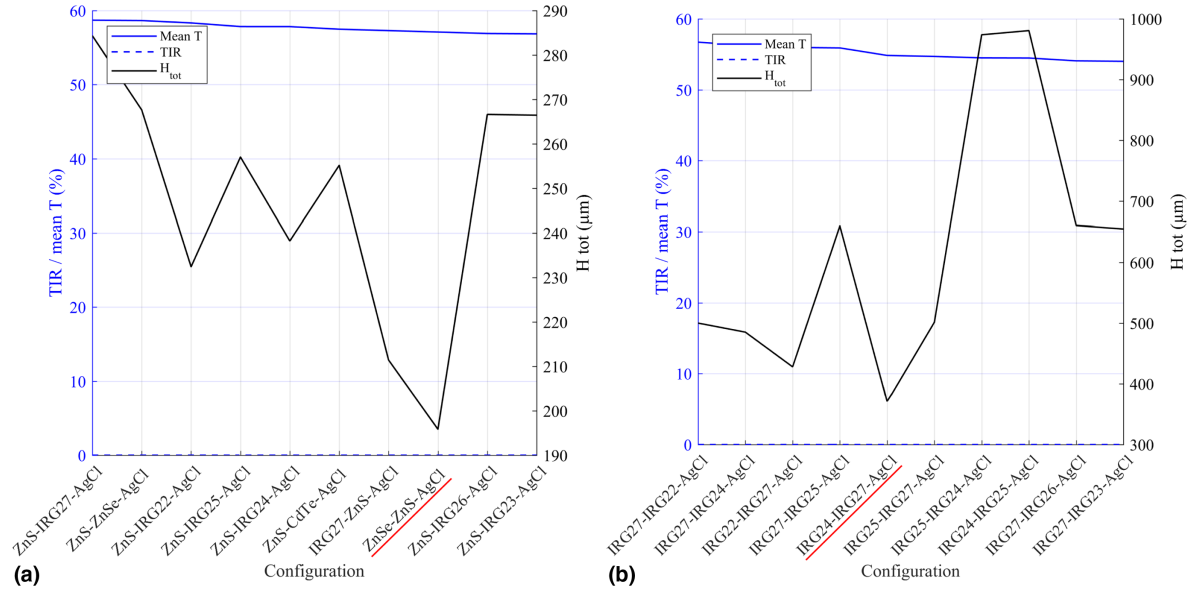

Fig. 6. On-axis geometric selection method results for the 10 "best" material configurations with all layer/gap material variables. The design parameters are $D = 10$ mm, F/15, and $N = 10$. Three evaluation metrics are shown: transmission (blue line, left axis), TIR (blue dotted line, left axis) and thickness (black line, right axis). The best MLDOE combinations are underlined in red and correspond to the solutions with the lowest TIR and thickness and with high transmission. (a) All IR materials and (b) "soft" materials.

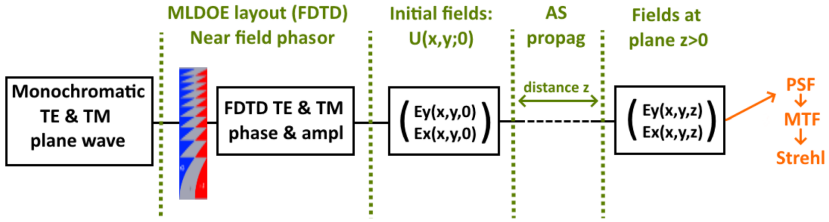

Fig. 7. Numerical simulation process to evaluate the MLDOE optical performance (PSF, MTF, Strehl ratio). An input plane wave is delayed due to the MLDOE, and the resulting vectorial near field is computed using the rigorous FDTD method. This input field ($z = 0$) is propagated to any plane $z > 0$ along the optical axis using the Fourier optics angular spectrum, generating a vectorial output field. The "best" focal plane is defined as the plane providing the highest Strehl ratio value, where optical metrics are generated. Adapted from [16].

GO-MSM. We use the Strehl ratio as an evaluation metric, computed at the best focal plane. FDTD rigorous wave simulation is performed using OptiFDTD software [25]. Starting from a plane wave, a complex electric field is propagated numerically through the MLDOE. Only the E_x and E_y components are considered, the E_z component being negligible, as it is along the propagation direction. The circular symmetry of the problem is used to reduce the sampling effort needed.

The resulting vectorial optical field obtained in the MLDOE near field is $E(x, y) = [E_x(x, y); E_y(x, y)]$. The E_x and E_y components are obtained respectively through separate transverse magnetic and transverse electric polarization simulations, and therefore they are not coupled. These two components can be propagated using the angular spectrum in free space [26] and incoherently summed to obtain the point spread function (PSF), modulation transfer function, and Strehl ratio at the target plane, meaning that the simulation is done for unpolarized light. This simulation process is described in Fig. 7, adapted from [16].

The hybrid process displayed in Fig. 7 is used in this section to study the output performance of MLDOE designs obtained with the PIDE-MSM and with the proposed GO-MSM. The aim is not to compare MLDOE combinations between them but rather to analyze whether their resulting optical performances were expected by the GO-MSM or the PIDE-MSM.

Practically, the Strehl ratio at the best focal plane is computed using the Fig. 7 procedure for the optimal results of each approach: IRG24-Air-IRG25 and IRG22-IRG25-CdTe (PIDE-MSM), ZnS-Air-Ge and IRG24-Air-IRG27 (two-layer DOE GO-MSM), ZnSe-ZnS-AgCl and IRG24-IRG27-AgCl (three-layer DOE GO-MSM). For each of the six combinations, multiple FDTD calculi have been made to obtain the polychromatic variation of the Strehl ratio. As stated in Sections 4.A and 4.B, the input design parameters are the same for all MLDOE combinations: $D = 10$ mm, F/15, and $N = 10$.

Figure 8 shows the polychromatic evolution of the Strehl ratio for the MLDOE design solutions mentioned above.

Figure 8 displays the six best MLDOE material combinations obtained using the GO-MSM and the PIDE-MSM. The IRG24-Air-IRG27 configuration, resulting from Fig. 5(b), has a polychromatic Strehl ratio of less than 5%, which is in

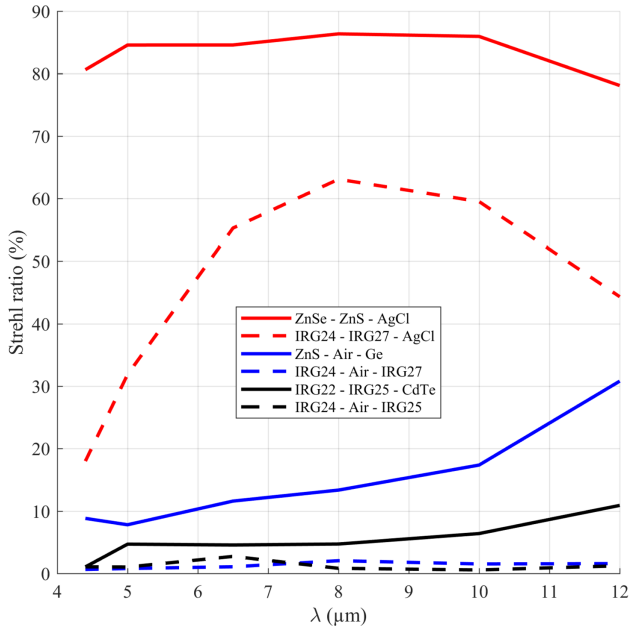

Fig. 8. Polychromatic evolution of the Strehl ratio, computed at the "best" focal plane (following the procedure described in Fig. 7). The "optimal" combinations obtained with the PIDE-MSM and GO-MSM are displayed: PIDE-MSM (black curves, Fig. 2), GO-MSM with two-layer DOEs (blue curves, Fig. 5), and GO-MSM with three-layer DOEs (red curves, Fig. 6). The polychromatic Strehl ratios of the PIDE-MSM solutions are worse than predicted in Fig. 2.

agreement with its very low transmission, and very high TIR and thickness. Similarly, the ZnS-air-Ge configuration also performs poorly, as expected by its transmission value of only 22% in Fig. 5(a).

The two optimal three-layer DOEs configurations, ZnSe-ZnS-AgCl and IRG24-IRG27-AgCl, resulting from Fig. 6, display a relatively high performance for all wavelengths, especially ZnSe-ZnS-AgCl. They both provide ∼60% transmission and no TIR, but the thickness of ZnSe-ZnS-AgCl is around 200 μm [Fig. 6(a)], while it is nearly double for the IRG24-IRG27-AgCl configuration [Fig. 6(b)], explaining its lower polychromatic Strehl ratio.

Finally, looking back at Figs. 2(a) and 2(b), both IRG24-Air-IRG25 and IRG22-IRG25-CdTe combinations provide extremely high PIDE values (around 99% on-axis). This result does not concur with the black curves displayed in Fig. 8. The fact that the TEA does not account for transmission losses and TIR (as pointed out in Section 2.C) entails too optimistic results for the PIDE method.

A clear link arises between the GO-MSM metrics (transmission, TIR, thickness) and the polychromatic performance at the focal plane. An MLDOE combination with high transmission, null TIR, and low thickness (ZnSe-ZnS-AgCl) tends to present a high polychromatic Strehl ratio. Inversely, very thick MLDOEs present high TIR and may perform very poorly. Consequently, this study shows the high potential of the GO-MSM when designing MLDOEs.

6. RESULTS DISCUSSION

It has been shown in this paper that the PIDE metric is not a reliable tool for the study and selection of MLDOEs. Thereby, PIDE calculation does not consider any refraction effect, thus neglecting transmission losses at optical interfaces (Fresnel reflection) and TIR. According to the phase expression in Eq. (1), the least angle-dependent combinations are obtained when the refractive indices of each layer are very close (with no dependency on the gap material), such as IRG24-Air-IRG25. On the other hand, the zone height design, based on Eq. (2), leads to very thick MLDOE combinations, which are more likely to encounter TIR. Therefore, the "thickness" metric is of prime importance, as it defines the susceptibility of an MLDOE to generate TIR, which strongly impacts its transmission.

Figure 8 clearly shows the performance difference between MLDOE combinations with and without an air gap. Due to sharper refractive index transitions between interfaces, the air gap (or any low index gap material) potentially decreases MLDOE imaging performance. To be performing, an MLDOE might require a filling material with a relatively high index to avoid TIR and enhance its IR transmission. High index materials, such as ZnS or ZnSe, tend to decrease the thickness of MLDOEs and provide valuable combinations. On the other hand, these materials are more difficult and expensive to manufacture, due to their hardness.

Although three-layer DOEs might be difficult to manufacture and two-layer DOEs seem to perform poorly (Fig. 5), MLDOEs are still very useful dual-band IR components. Thereby, using different groove design models such as the extended scalar theory [27,28] or the effective area method [13,14], the performance of two-layer DOEs might increase tremendously, since these methods tend to lower the aspect ratio of extreme zones, limiting TIR.

Finally, we mention that for the design of a hybrid dual-band system, the GO-MSM method can be used as an iterative process where the materials as well as the MLDOE parameters (diameter, number of zones, focal length) can vary. Thereby, design achromatization adds constraints to the GO-MSM that are not taken into account in this paper. In addition, manufacturing constraints must also be considered to enhance the presented method.

7. CONCLUSION

The proposed GO-MSM, based on TIR, transmission, and thickness, can provide optically performing solutions. In addition, it is fast and reliable and does not require time-consuming wave simulations, except for the validation of the results. Therefore, it is a valuable optimization tool. Rigorous wave propagation has been used to validate the results of the GO-MSM, which has proven to perform much better than the PIDE-MSM in the frame of the studied thick MLDOEs.

This study has also highlighted the benefit of adding a high index gap material to reduce the TIR and enhance the optical performance.

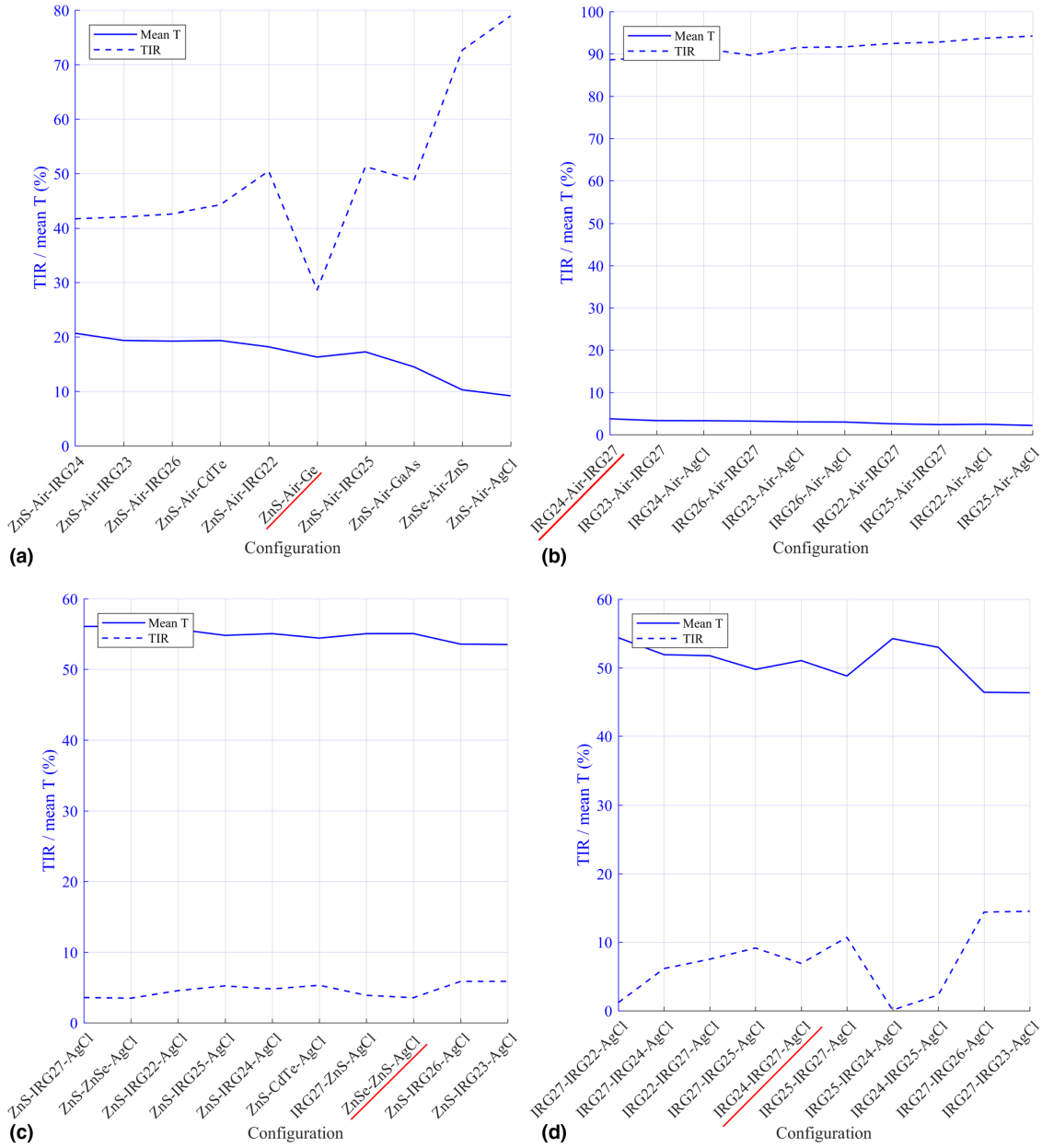

Fig. 9. Off-axis geometric selection method results for the 10 "best" material configurations considering: (a) two-layer DOEs, all IR materials, (b) two-layer DOEs, "soft" materials, (c) three-layer DOEs, all IR materials, and (d) three-layer DOEs, soft materials. The same materials and x-label configuration have been kept from Figs. 5 and 6 to ease the comparison. The design parameters are $D = 10$ mm, F/15, and $N = 10$. Three evaluation metrics are shown: transmission (blue line, left axis), TIR (blue dotted line, left axis), and thickness (black line, right axis). The best MLDOE combinations selected in Figs. 5 and 6 are underlined in red.

APPENDIX A

In this section, the same optimizations as in Sections 4.A and 4.B are performed with an incident angle of 15°. The results are displayed in Fig. 9. Figures 9(a)–9(d) respectively correspond to an off-axis version of Figs. 5(a), 5(b), 6(a), and 6(b).

As a result of Fig. 9, an increase in TIR is noticed, especially in (a) and (d), but they have no impact on the selected configurations of Sections 4.A and 4.B. The thickness is not depicted here since it does not change when off-axis incidence is considered. In Fig. 9(d), IRG24-IRG27-AgCl is still considered the best combination since it has the lowest thickness, but IRG24-IRG27-AgCl also appears as a very good solution.

Disclosures. The authors declare no conflicts of interest.

Data availability. No data were generated or analyzed in the presented research.

REFERENCES

1. J. A. Sobrino, F. Del Frate, M. Drusch, J. C. Jimenez-Munoz, P. Manunta, and A. Regan, "Review of thermal infrared applications and requirements for future high-resolution sensors," IEEE Trans. Geosci. Remote Sens. **54**, 2963–2972 (2016).
2. J. A. Sobrino, F. Del Frate, M. Drusch, J. C. Jimenez-Munoz, and P. Manunta, *Review of High Resolution Thermal Infrared Applications*

and Requirements: The Fuegosat Synthesis Study (Springer, 2013), vol. **17**.
3. SCHOTT, "Reliable solutions for the infrared industry," 2020, https://www.schott.com/advanced_optics/english/products/optical-materials/ir-materials/infrared-chalcogenide-glasses/index.html.
4. Y. Arieli, S. Noach, S. Ozeri, and N. Eisenberg, "Design of diffractive optical elements for multiple wavelengths," Appl. Opt. **37**, 6174–6177 (1998).
5. C. W. Sweeney and G. E. Sommargren, "Harmonic diffractive lenses," Appl. Opt. **34**, 2469–2475 (1995).
6. D. Faklis and G. M. Morris, "Spectral properties of multiorder diffractive lenses," Appl. Opt. **34**, 2462–2468 (1995).
7. C. Fan, Z. Wang, L. Lin, M. Zhang, and H. Fan, "Design of infrared telephoto-optical system with double layer harmonic diffractive element," Chin. Phys. Lett. **24**, 1973–1976 (2007).
8. C. Xue, Q. Cui, T. Liu, Y. Liangliang, and B. Fei, "Optimal design of multilayer diffractive optical element for dual wavebands," Opt. Lett. **35**, 4157–4159 (2010).
9. S. Mao, Q. Cui, M. Piao, and L. Zhao, "High diffraction efficiency of three-layer diffractive optics designed for wide temperature range and large incident angle," Appl. Opt. **55**, 3549–3554 (2016).
10. B. Zhang, Q. Cui, and M. Piao, "Effect of substrate material selection on polychromatic integral diffraction efficiency for multilayer diffractive optics in oblique incident situation," Opt. Commun. **415**, 156–163 (2018).
11. T. Wang, H. Liu, H. Zhang, H. Zhang, Q. Sun, and Z. Lu, "Effect of incidence angles and manufacturing errors on the imaging performance of hybrid systems," J. Opt. **13**, 035711 (2011).
12. H. Yang, C. Xue, C. Li, J. Wang, and R. Zhang, "Diffraction efficiency sensitivity to oblique incident angle for multilayer diffractive optical elements," Appl. Opt. **55**, 7126–7133 (2016).
13. H. Yang, C. Xue, C. Li, and J. Wang, "Optimal design of multilayer diffractive optical elements with effective area method," Appl. Opt. **55**, 1675–1682 (2016).
14. C. Yang, H. Yang, C. Li, and C. Xue, "Optimization and analysis of infrared multilayer diffractive optical elements with finite feature sizes," Appl. Opt. **58**, 2589–2595 (2019).
15. F. Wyrowski and M. Kuhn, "Introduction to field tracing," J. Mod. Opt. **58**, 449–466 (2010).
16. V. Laborde, J. Loicq, J. Hastanin, and S. Habraken, "Hybrid ray-tracing/Fourier optics method to analyze multilayer diffractive optical elements," Appl. Opt. **61**, 4956–4966 (2022).
17. D. A. Buralli and G. M. Morris, "Effects of diffraction efficiency on the modulation transfer function of diffractive lenses," Appl. Opt. **31**, 4389–4396 (1992).
18. H. Zhong, S. Zhang, F. Wyrowski, and H. Schweitzer, "Parabasal thin element approximation for the analysis of the diffractive optical elements," Proc. SPIE **9131**, 278–291 (2014).
19. V. Moreno, J. R. Salgueiro, and J. F. Román, "High efficiency diffractive lenses: deduction of kinoform profile," Am. J. Phys. **65**, 556–562 (1997).
20. D. A. Pommet, M. Moharam, and E. B. Grann, "Limits of scalar diffraction theory for diffractive phase elements," J. Opt. Soc. Am. **11**, 1827–1834 (1994).
21. G. Greisukh, G. Danilov, E. Ezhov, S. Stepanov, and B. Usievich, "Comparison of electromagnetic and scalar methods for evaluation of efficiency of diffractive lenses for wide spectral bandwidth," Opt. Commun. **338**, 54–57 (2015).
22. H. Sauer, P. Chavel, and G. Erdei, "Diffractive optical elements in hybrid lenses: modeling and design by zone decomposition," Appl. Opt. **38**, 6482–6486 (1999).
23. A. Nemes-Czopf, D. Bercsényi, and G. Erdei, "Simulation of relief-type diffractive lenses in ZEMAX using parametric modelling and scalar diffraction," Appl. Opt. **58**, 8931–8942 (2019).
24. Breault Research Organization, "ASAP NextGen," 2022, https://breault.com/asap/.
25. Optiwave Photonic Software, "OptiFDTD," 2022, https://optiwave.com/optifdtd-overview/.
26. J. W. Goodman, "The angular spectrum of plane waves," in *Introduction to Fourier Optics* (McGraw-Hill, 1996), Chap. 3.
27. F. Huo, W. Wang, and C. Xue, "Limits of scalar diffraction theory for multilayer diffractive optical elements," Optik **127**, 5688–5694 (2016).
28. G. Swanson, "Binary optics technology: theoretical limits on the diffraction efficiency of multilevel diffractive optical elements," Technical Report (Lincoln Laboratory, Massachusetts Institute of Technology, 1991).